

Parton Distribution Function Nuclear Corrections for Charged Lepton and Neutrino Deep Inelastic Scattering Processes

I. Schienbein,^{1,*} J. Y. Yu,^{2,†} K. Kovařík,^{1,‡} C. Keppel,^{3,4,§}
 J. G. Morfín,^{5,¶} F. I. Olness,^{2,**} and J.F. Owens^{6,††}

¹*Laboratoire de Physique Subatomique et de Cosmologie, Université Joseph Fourier/CNRS-IN2P3/INPG,
 53 Avenue des Martyrs, 38026 Grenoble, France*

²*Southern Methodist University, Dallas, TX 75275, USA*

³*Thomas Jefferson National Accelerator Facility, Newport News, VA 23602, USA*

⁴*Hampton University, Hampton, VA, 23668, USA*

⁵*Fermilab, Batavia, IL 60510, USA*

⁶*Florida State University, Tallahassee, FL 32306-4350, USA*

We perform a χ^2 -analysis of Nuclear Parton Distribution Functions (NPDFs) using neutral current charged-lepton ($\ell^\pm A$) Deeply Inelastic Scattering (DIS) and Drell-Yan data for several nuclear targets. The nuclear A dependence of the NPDFs is extracted in a next-to-leading order fit. We compare the nuclear corrections factors (F_2^{Fe}/F_2^D) for this charged-lepton data with other results from the literature. In particular, we compare and contrast fits based upon the charged-lepton DIS data with those using neutrino-nucleon DIS data.

PACS numbers: 12.38.-t,13.15.+g,13.60.-r,24.85.+p

Keywords: Nuclear PDF, PDF, DIS, Drell-Yan

Contents

I. Introduction	1
A. PDFs and Nuclear Corrections	1
B. Nuclear Corrections in the Literature	2
C. Outline	2
II. NPDF Global Analysis Framework	2
A. PDF analysis framework	2
B. Inputs to the Global NPDF Fit	4
C. Result of the NPDF Fit	4
III. $\ell^\pm A$ Nuclear Corrections	5
A. Charged-Lepton ($\ell^\pm A$) Data	5
IV. $\ell^\pm A$ and νA Nuclear Corrections	5
A. Nuclear Corrections in νA DIS	5
B. $\ell^\pm A$ and νA Comparison	5
V. Conclusions	7
Acknowledgment	7
References	7

I. INTRODUCTION

A. PDFs and Nuclear Corrections

Parton distribution functions (PDFs) are of supreme importance in contemporary high energy physics as they are needed for the computation of reactions involving hadrons based on QCD factorization theorems [1–3]. For this reason various groups present global analyses of PDFs for protons [4–11] and nuclei [12–17] which are regularly updated in order to meet the increasing demand for precision. The PDFs are non-perturbative objects which must be determined by experimental input. To fully constrain the x -dependence and flavor-dependence of the PDFs requires large data sets from different processes which typically include Deeply Inelastic Scattering (DIS), Drell–Yan (DY), and jet production.

While some of this data is extracted from free protons, much is taken from a variety of nuclear targets. Because the neutrino cross section is so small, to obtain sufficient statistics for the neutrino-nuclear DIS processes it is necessary to use massive targets (*e.g.*, iron, lead, etc.). Therefore, nuclear corrections are required if we are to include the heavy target data into the global analysis of proton PDFs.

The heavy target neutrino DIS data plays an important role in extracting the separate flavor components of the PDFs. In particular, this data set gives the most precise information on the strange quark PDF. As the strange quark uncertainty may limit the precision of particular Large Hadron Collider (LHC) W and Z measurements, the nuclear corrections and their uncertainties will have a broad impact on a comprehensive understanding of current and future data sets.

*schien@lpsc.in2p3.fr

†yu@physics.smu.edu

‡kovarik@lpsc.in2p3.fr

§keppel@jlab.org

¶morfín@fnal.gov

**olness@smu.edu

††owens@hep.fsu.edu

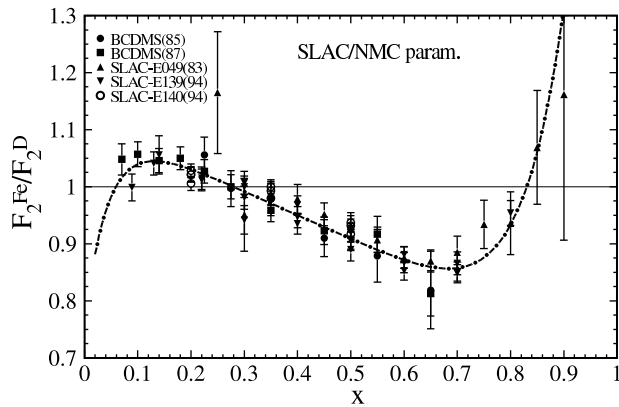


Figure 1: Nuclear correction ratio, F_2^{Fe}/F_2^D , as a function of x . The parameterized curve is compared to SLAC and BCDMS data [18–24].

B. Nuclear Corrections in the Literature

In previous PDF analyses [25, 26], a fixed nuclear correction was applied to “convert” the data from a heavy target to a proton. As such, these nuclear correction factors were frozen at a fixed value. They did not adjust for the Q^2 scale or the physical observable (F_2 , F_3 , $\frac{d\sigma}{dx dy}$), and they did not enter the PDF uncertainty analysis.

While this approach may have been acceptable in the past given the large uncertainties, improvements in both data and theory precision demand comparable improvements in the treatment of the nuclear corrections.

Figure 1 displays the F_2^{Fe}/F_2^D structure function ratio as measured by the SLAC and BCDMS collaborations. The SLAC/NMC curve is the result of an A -independent parameterization fit to calcium and iron charged-lepton DIS data [18–24, 27]. This parameterization was used to “convert” heavy target data to proton data, which then would be input into the global proton PDF fit.¹ The SLAC/NMC parameterization was then applied to *both* charged-lepton–nucleus and neutrino–nucleus data, and this correction was taken to be independent of the scale Q and the specific observable $\{F_2, F_3, \dots\}$. Recent work demonstrates that the parameterized approximation of Fig. 1 is not sufficient and it is necessary to account for these details [28–30].

C. Outline

In this paper, we present a new framework for a global analysis of nuclear PDFs (NPDFs) at Next-to-Leading-

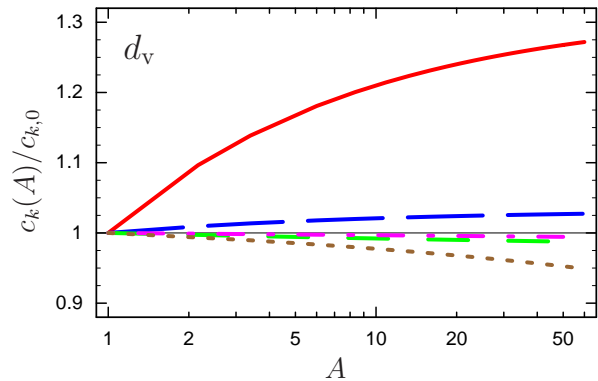
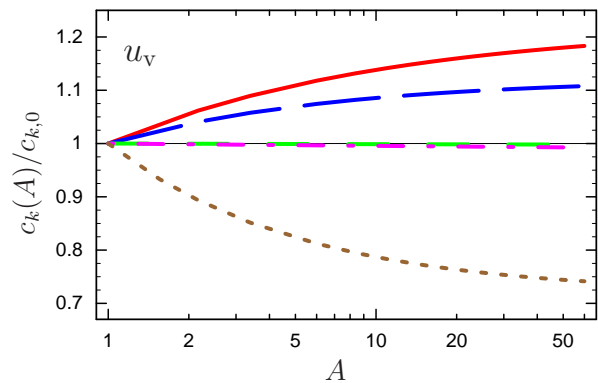


Figure 2: We display the A -dependent coefficients $c_k(A)$, $k = \{1, 5\}$, for the up-valence (top) and down-valence PDF (bottom) as a function of the nuclear A . The dependence of the coefficients $c_k(A)$ is shown by the following lines: c_1 - solid (red) line, c_2 - long dashed (blue) line, c_3 - dashed (green) line, c_4 - dash-dotted (magenta) line, c_5 - dotted (brown) line.

Order (NLO). An important and appealing feature of this framework is that it naturally extends the proton analysis by endowing the free fit parameters with a dependence on the atomic number A . This will allow us to study proton and nuclear PDFs simultaneously such that nuclear correction factors needed for the proton analysis can be computed dynamically.

In Section II, we outline our method for the analysis, specify the DIS and DY data sets, and present the χ^2 of our fit. In Section III, we compute the nuclear correction factors (F_2^{Fe}/F_2^D) for the fit to the $\ell^\pm A$ and DY data. In Section IV, we compare these results to the nuclear correction factors (F_2^{Fe}/F_2^D) from the νA fit of Ref. [30]. Finally, we summarize our results in Section V.

II. NPDF GLOBAL ANALYSIS FRAMEWORK

A. PDF analysis framework

In this section, we present the global analysis of NPDFs using charged-lepton DIS ($\ell^\pm A$) and Drell–Yan data to extend the analysis of Ref. [27] for a variety of nuclear

¹ Technically, the heavy target data was scaled to a deuteron target, and then isospin symmetry relations were used to obtain the corresponding proton data. Deuteron corrections were used in certain cases.

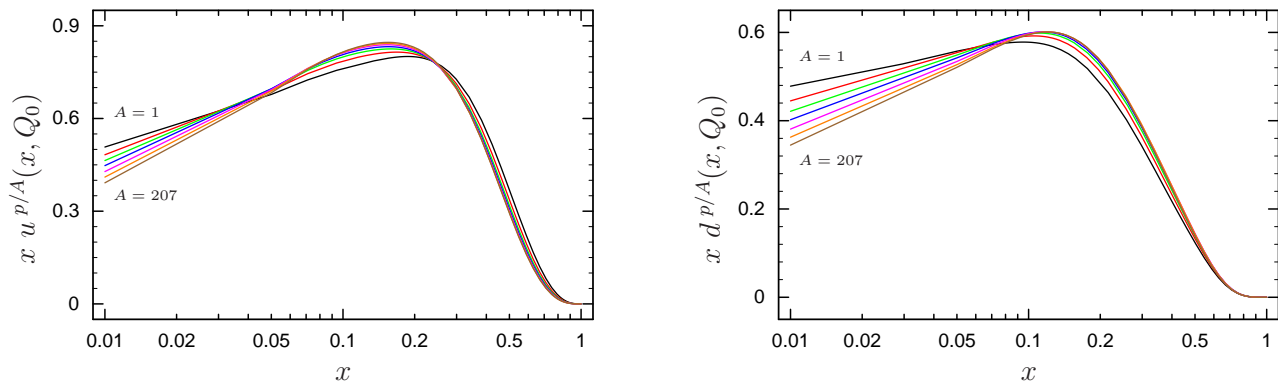


Figure 3: We display the a) $xu(x)$ and b) $xd(x)$ PDFs for a selection of nuclear A values ranging from $A = \{1, 207\}$. We choose $Q_0 = 1.3$ GeV. The different curves depict the PDFs of nuclei with the following atomic numbers (from top to bottom at $x = 0.01$) $A = 1, 2, 4, 8, 20, 54,$ and 207 .

targets. This analysis is performed in close analogy with what is done for the $A = 1$ free proton case [45]. We will use the general features of the QCD-improved parton

model and the χ^2 analyses as outlined in Ref. [30]. The input distributions are parameterized as

$$\begin{aligned} x f_k(x, Q_0) &= c_0 x^{c_1} (1-x)^{c_2} e^{c_3 x} (1+e^{c_4 x})^{c_5} & k = u_v, d_v, g, \bar{u} + \bar{d}, s, \bar{s}, \\ \bar{d}(x, Q_0)/\bar{u}(x, Q_0) &= c_0 x^{c_1} (1-x)^{c_2} + (1+c_3 x)(1-x)^{c_4}, \end{aligned} \quad (1)$$

at the scale $Q_0 = 1.3$ GeV. Here, the u_v and d_v are the up- and down-quark valence distributions, \bar{u} , \bar{d} , s , \bar{s} are the anti-up, anti-down, strange and anti-strange sea distributions, and g is the gluon.

In order to accommodate different nuclear target materials, we introduce a nuclear A -dependence in the c_k coefficients:

$$c_k \rightarrow c_k(A) \equiv c_{k,0} + c_{k,1} (1 - A^{-c_{k,2}}), \quad k = \{1, \dots, 5\}. \quad (2)$$

This ansatz has the advantage that in the limit $A \rightarrow 1$ we have $c_k(A) \rightarrow c_{k,0}$; hence, $c_{k,0}$ is simply the corresponding coefficient of the free proton. Thus, we can relate the $c_{k,0}$ parameters to the analogous quantities from proton PDF studies.

It is noteworthy that the x -dependence of our input distributions $f_k^{p/A}(x, Q_0)$ is the same for all nuclei A ; hence, this approach treats the NPPDFs and the proton PDFs on the same footing.² Additionally, this method facilitates the interpretation of the fit at the parameter level by allowing us to study the $c_k(A)$ coefficients as

functions of the nuclear A parameter.

With this A -generalized set of initial PDFs, we can apply the DGLAP evolution equations to obtain the PDFs for a bound neutron inside a nucleus A , $f_i^{n/A}(x, Q)$. We can then construct the PDFs for a general (A, Z) -nucleus:

$$f_i^{(A,Z)}(x, Q) = \frac{Z}{A} f_i^{p/A}(x, Q) + \frac{(A-Z)}{A} f_i^{n/A}(x, Q) \quad (3)$$

where we relate the distributions of a bound neutron, $f_i^{n/A}(x, Q)$, to those of a proton by isospin symmetry. Similarly, the nuclear structure functions are given by:

$$F_i^{(A,Z)}(x, Q) = \frac{Z}{A} F_i^{p/A}(x, Q) + \frac{(A-Z)}{A} F_i^{n/A}(x, Q). \quad (4)$$

These structure functions can be computed at next-to-leading order as convolutions of the nuclear PDFs with the conventional Wilson coefficients, *i.e.*, generically

$$F_i^{(A,Z)}(x, Q) = \sum_k C_{ik} \otimes f_k^{(A,Z)}. \quad (5)$$

² The nuclear analogue of the scaling variable x is defined as $x := Ax_A$ where $x_A = Q^2/2P_A \cdot q$ is the usual Bjorken variable formed out of the four-momenta of the nucleus (P_A) and the exchanged boson (q), with $Q^2 = -q^2$ [30].

To account for heavy quark mass effects, we calculate the relevant structure functions in the Aivazis-Collins-Olness-Tung (ACOT) scheme [46, 47] at NLO QCD [48].

F_2^A/F_2^D :			
Observable	Experiment	Ref.	# data
D	NMC-97	[31]	275
He/D	SLAC-E139	[18]	18
	NMC-95,re	[32]	16
	Hermes	[33]	92
Li/D	NMC-95	[34]	15
Be/D	SLAC-E139	[18]	17
C/D	EMC-88	[35]	9
	EMC-90	[36]	2
	SLAC-E139	[18]	7
	NMC-95,re	[32]	16
	NMC-95	[34]	15
	FNAL-E665-95	[37]	4
N/D	BCDMS-85	[19]	9
	Hermes	[33]	92
Al/D	SLAC-E049	[38]	18
	SLAC-E139	[18]	17
Ca/D	EMC-90	[36]	2
	SLAC-E139	[18]	7
	NMC-95,re	[32]	15
	FNAL-E665-95	[37]	4
Fe/D	BCDMS-85	[19]	6
	BCDMS-87	[20]	10
	SLAC-E049	[21]	14
	SLAC-E139	[18]	23
	SLAC-E140	[22]	6
Cu/D	EMC-88	[35]	9
	EMC-93(addendum)	[39]	10
	EMC-93(chariot)	[39]	9
Kr/D	Hermes	[33]	84
Ag/D	SLAC-E139	[18]	7
Sn/D	EMC-88	[35]	8
Xe/D	FNAL-E665-92(em cut)	[40]	4
Au/D	SLAC-E139	[18]	18
Pb/D	FNAL-E665-95	[37]	4
Total:			862

Table I: The DIS F_2^A/F_2^D data sets used in the fit. The table details the specific nuclear targets, references, and the number of data points without kinematical cuts.

B. Inputs to the Global NPDF Fit

Using the above framework, we can then construct a global fit to charged-lepton–nucleus ($l^\pm A$) DIS data and Drell–Yan data. To guide our constraints on the $c_{k,0}$ coefficients, we use the global fit of the proton PDFs based upon Ref. [27]. This fit has the advantage that the extracted proton PDFs have minimal influence from nuclear targets. To provide the A -dependent nuclear information, we use a variety of $l^\pm A$ DIS data and Drell–Yan data. The complete list of nuclear targets and processes

$F_2^A/F_2^{A'}$:			
Observable	Experiment	Ref.	# data
Be/C	NMC-96	[41]	15
Al/C	NMC-96	[41]	15
Ca/C	NMC-95	[32]	20
	NMC-96	[41]	15
Fe/C	NMC-95	[41]	15
Sn/C	NMC-96	[42]	144
Pb/C	NMC-96	[41]	15
C/Li	NMC-95	[32]	20
Ca/Li	NMC-95	[32]	20
Total:			279

Table II: The DIS $F_2^A/F_2^{A'}$ data sets used in the fit. The table details the specific nuclear targets, references, and the number of data points without kinematical cuts.

$\sigma_{DY}^{pA}/\sigma_{DY}^{pA'}$:			
Observable	Experiment	Ref.	# data
C/D	FNAL-E772-90	[43]	9
Ca/D	FNAL-E772-90	[43]	9
Fe/D	FNAL-E772-90	[43]	9
W/D	FNAL-E772-90	[43]	9
Fe/Be	FNAL-E866-99	[44]	28
W/Be	FNAL-E866-99	[44]	28
Total:			92

Table III: The Drell-Yan data sets used in the fit. The table details the specific nuclear targets, references, and the number of data points without kinematical cuts.

is listed in Tables I, II, and III; there are 1233 data points before kinematical cuts are applied.

The structure of the fit is analogous to that of Ref. [30]. For the quark masses we take $m_c = 1.3$ GeV and $m_b = 4.5$ GeV. To limit effects of higher-twist we choose standard kinematic cuts of $Q_{cut} = 2.0$ GeV, and $W_{cut} = 3.5$ GeV as they are employed in the CTEQ proton analyses.³ There are 708 data points which satisfy these cuts. The fit was performed with 32 free parameters which gives 676 degrees of freedom (dof).

C. Result of the NPDF Fit

Performing the global fit to the data, we obtain an overall χ^2/dof of 0.946. Individually, we find a χ^2/pt of 0.919 for the F_2^A/F_2^D measurements of Table I, of 0.685 for the $F_2^A/F_2^{A'}$ measurements of Table II, and of 1.077

³ For example, see the CTEQ (Coordinated Theoretical-Experimental project on QCD) analysis of Ref. [45] which presents the CTEQ6 PDF sets.

for the Drell–Yan measurements of Table III. The fact that we obtain a good fit implies that we have devised an efficient parameterization of the underlying physics.

The output of the fit is the set of $c_{k,i}$ parameters and a set of A -dependent momentum fractions for the gluon and the strange quark. Using the $c_{k,i}$ coefficients we can construct the A -dependent $c_k(A)$ functions which determine the nuclear PDFs at the initial Q_0 scale: $f_i^A(x, Q_0)$. As an example, we display the $c_k(A)$ functions in Fig. 2 for the case of the up-valence and down-valence distributions.

Finally, we can use the DGLAP evolution equations to evolve to an arbitrary Q to obtain the desired $f_i^A(x, Q)$ functions. In Fig. 3 we display the up- and down-quark PDFs at a scale of $Q_0 = 1.3$ GeV as a function of x for a variety of nuclear- A values.

III. $\ell^\pm A$ NUCLEAR CORRECTIONS

Nuclear corrections are the key elements which allow us to combine data across different nuclear targets and provide maximum information on the proton PDFs. As the nuclear target data plays a critical role in differentiating the separate partonic flavors (especially the strange quark), this data provides the foundation that we will use to make predictions at the LHC.

A. Charged-Lepton ($\ell^\pm A$) Data

The present nuclear PDF global analysis provides us with a complete set of NPDFs $f_i^A(x, Q)$ with full functional dependence on $\{x, Q, A\}$. Consequently, the traditional nuclear correction F_2^{Fe}/F_2^D does not have to be applied as a “frozen” external factor, but can now become a dynamic part of the fit which can be adjusted to accommodate the various data sets.

Having performed the fit outlined in Sec. II, we can then use the $f_i^A(x, Q)$ to construct the corresponding quantity F_2^{Fe}/F_2^D to find the form that is preferred by the data. In order to construct the ratio, we use the expression given by Eq. 4 for iron and deuterium. This result is displayed in Figure 4-a) for a scale of $Q^2 = 5$ GeV², and in Figure 5-a) for a scale of $Q^2 = 20$ GeV². Comparing these figures, we immediately note that our ratio F_2^{Fe}/F_2^D has non-trivial Q -dependence—as it should.

Figures 4-a) and 5-a) also compare our extracted F_2^{Fe}/F_2^D ratio with the (Q -independent) SLAC/NMC parameterization of Figure 1 and with the fits from Kulagin-Petti (KP) [28, 29] and Hirai-Kumano-Nagai (HKN07) [12]. We observe that in the intermediate range ($x \in \sim [0.07, 0.7]$) where the bulk of the SLAC/NMC data constrains the parameterization, our computed F_2^{Fe}/F_2^D ratio compares favorably. When comparing the different curves, one has to bear in mind the following two points. First, all curves in principle have an uncertainty band

which is not shown. Second, the data points used to extract the SLAC/NMC curve are measured at different Q^2 whereas our curve is always at a fixed $Q^2 = 5$ GeV² or $Q^2 = 20$ GeV². In light of these facts, we conclude that our fit agrees very well with other models and parametrizations as well as with the measured data points.

It should be noted that the kinematic cuts we employed to avoid higher twist effects effectively exclude all data points in the high- x region above $x \gtrsim 0.7$. This is reflected by the fact that our curves in Figs. 4-a) and 5-a) stop at $x = 0.7$. The high- x region is beyond the scope of this paper and will be subject of a future analysis.

Thus, we find that data sets used in this fit (F_2^A/F_2^D , $F_2^A/F_2^{A'}$, and $\sigma_{DY}^{pA}/\sigma_{DY}^{pA'}$) are compatible with the SLAC, BCDMS, and NMC data. Additionally, we can go further and use our complete set of NPDFs $f_i^A(x, Q)$ to compute the appropriate nuclear correction not only for F_2^{Fe}/F_2^D , but for *any* nuclear target (A) for any Q -value, and for any observable. We make use of this property in the following section where we compute the corresponding quantity for a different nuclear process.

IV. $\ell^\pm A$ AND νA NUCLEAR CORRECTIONS

A. Nuclear Corrections in νA DIS

In a previous analysis [30], we examined the charged current (CC) neutrino–nucleus DIS process $\nu A \rightarrow \mu X$, and extracted the F_2^{Fe}/F_2^D ratio.⁴

These results are displayed in Figures 4-b) and 5-b). The solid line is the result of the global fit (fit A2), and this is compared with the previous SLAC/NMC parameterization, as well as fits KP and HKN07. The data points displayed come from the NuTeV experiment [49, 50]. The (yellow) band is an approximation of the uncertainty of the fits.

As observed above, the SLAC/NMC parameterization is generally consistent with the results of KP and HKN as well as our B fit to $\ell^\pm A$ and DY data. However, the A2 fit of Figures 4-b) and 5-b) does not agree with any of these three results. We now examine this in detail.

B. $\ell^\pm A$ and νA Comparison

The contrast between the charged-lepton ($\ell^\pm A$) case and the neutrino (νA) case is striking; while the charged-lepton results generally align with the SLAC/NMC, KP, and HKN determinations, the neutrino results clearly

⁴ While Ref. [30] extracted the nuclear PDFs using only the NuTeV neutrino–iron DIS data, Ref. [27] demonstrated that the Chorus neutrino–lead DIS data [51] was consistent with the NuTeV data set.

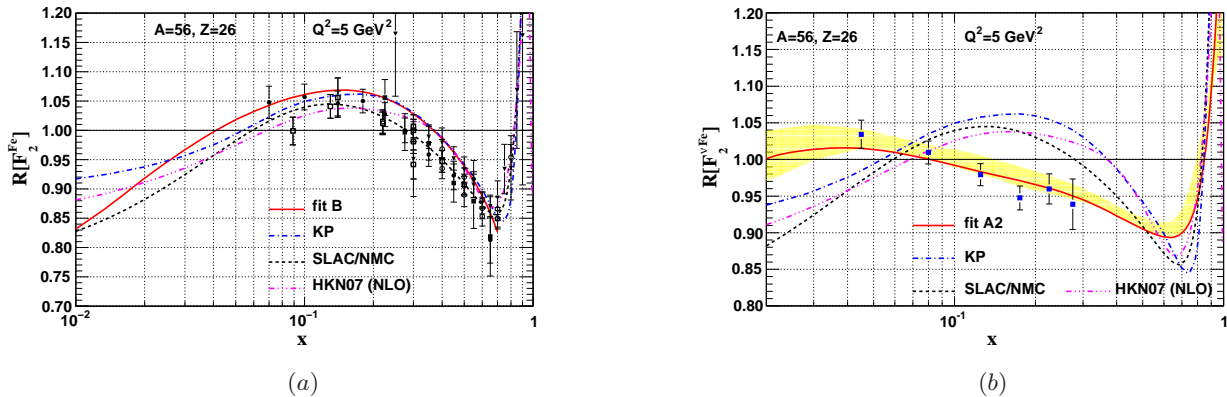


Figure 4: The computed nuclear correction ratio, $F_2^{F_e}/F_2^D$, as a function of x for $Q^2 = 5 \text{ GeV}^2$. Figure-a) shows the fit (fit B) using charged-lepton–nucleus ($\ell^\pm A$) and DY data whereas Figure-b) shows the fit using neutrino-nucleus (νA) data (fit A2 from Ref. [30]). Both fits are compared with the SLAC/NMC parameterization, as well as fits from Kulagin-Petti (KP) (Ref. [28, 29]) and Hirai *et al.* (HKN07), (Ref. [12]). The data points displayed in Figure-a) are the same as in Fig. 1 and those displayed in Figure-b) come from the NuTeV experiment [49, 50].

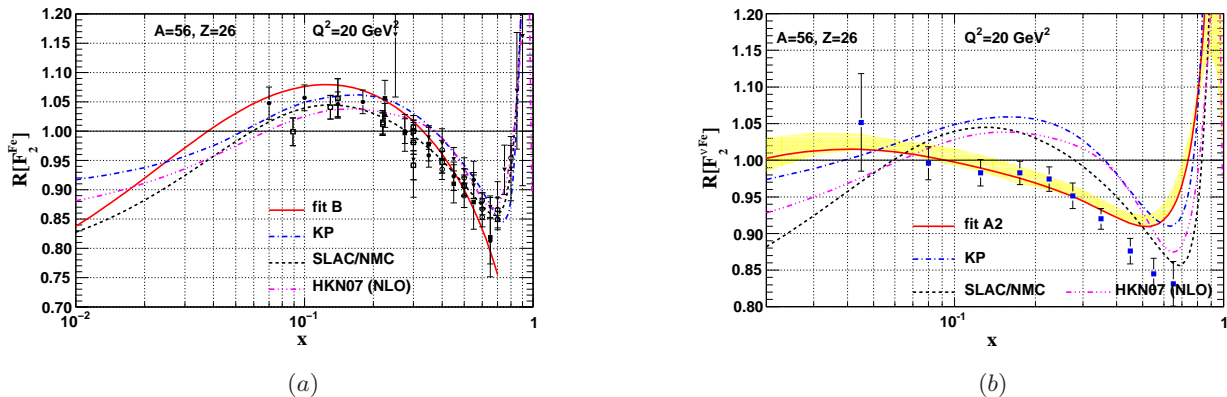


Figure 5: Same as Figure 4 for $Q^2 = 20 \text{ GeV}^2$.

yield different behavior in the intermediate x -region. We emphasize that both the charged-lepton and neutrino results are not a model—they come directly from global fits to the data. To emphasize this point, we have superimposed illustrative data point in Figures 4-b) and 5-b); these are simply the νA DIS data [49, 50] scaled by the appropriate structure function, calculated with the proton PDF of Ref. [30].

The mis-match between the results in charged-lepton and neutrino DIS is particularly interesting given that there has been a long-standing “tension” between the light-target charged-lepton data and the heavy-target neutrino data in the historical fits [52, 53]. This study demonstrates that the tension is not only between charged-lepton *light-target* data and neutrino heavy-target data, but we now observe this phenomenon in comparisons between neutrino and charged-lepton *heavy-target* data.

There are two possible interpretations of this result.

1. There is, in fact, a single “compromise” solution for

the $F_2^{F_e}/F_2^D$ nuclear correction factor which yields a good fit for both the νA and $\ell^\pm A$ data.

2. The nuclear corrections for the $\ell^\pm A$ and νA processes are different.

Considering possibility 1), the “apparent” discrepancy observed in Figures 4 and 5 could simply reflect uncertainties in the extracted nuclear PDFs. The global fit framework introduced in this work paves the way for a unified analysis of the $\ell^\pm A$, DY, and νA data which will ultimately answer this question. Having established the nuclear correction factors for neutrino and charged-lepton processes separately, we can combine these data sets (accounting for appropriate systematic and statistical errors) to obtain a “compromise” solution.⁵

⁵ While it is straightforward to obtain a “fit” to the combined neutrino and charged-lepton DIS data sets, determining the appro-

If it can be established that a “compromise” solution does not exist, then the remaining option is that the nuclear corrections in neutrino and charged-lepton DIS are different. This idea has previously been discussed in the literature [28, 29, 54]. We note that the charged-lepton processes occur (dominantly) via γ -exchange, while the neutrino-nucleon processes occur via W^\pm -exchange. Thus, the different nuclear corrections could simply be a consequence of the differing propagation of the intermediate bosons (photon, W) through dense nuclear matter. Regardless of whether this dilemma is resolved via option 1) or 2), understanding this puzzle will provide important insights about processes involving nuclear targets. Furthermore, a deeper understanding could be obtained by a future high-statistics, high-energy neutrino experiment using several nuclear target materials [55–57].

V. CONCLUSIONS

We presented a new framework to carry out a global analysis of NPDFs at next-to-leading order QCD, treating proton and nuclear targets on equal footing. Within this approach, we have performed a χ^2 -analysis of nuclear PDFs by extending the proton PDF fit of Ref. [27] to DIS $l^\pm A$ and Drell–Yan data. The result of the fit is a set of nuclear PDFs which incorporate not only the $\{x, Q\}$ -dependence, but also the nuclear- A degree of freedom; thus we can accommodate the full range of nuclear targets from light ($A = 1$) to heavy ($A = 207$). We find a good fit to the combined data set with a total χ^2/dof of 0.946 demonstrating the viability of the framework.

We have used our results to compute the nuclear corrections factors, and to compare these with the results from the literature. We find good agreement for those fits based on a charged-lepton data set.

Separately, we have compared our nuclear corrections (derived with a charged-lepton data set) with those computed using neutrino DIS ($\nu A \rightarrow \mu X$) data sets. Here, we observe substantive differences.

This fit is novel in several respects.

- Since we constructed the nuclear PDF fits analogous to the proton PDF fits, this framework allows

a meaningful comparison between these two distributions.

- The above unified framework integrates the nuclear correction factors as a dynamic component of the fit. These factors are essential if we want to use the heavy target DIS data to constrain the strange quark distribution of the proton, for example.
- This unified analysis of proton and nuclear PDFs provides the foundation necessary to simultaneously analyze $l^\pm A$, DY and, νA data. This will ultimately help in determining whether 1) a “compromise” solution exists, or 2) the nuclear corrections depend on the exchanged boson (e.g., γ/Z or W^\pm).

The compatibility of the charged-lepton $l^\pm A$ and neutrino-nucleus νA processes in the global analysis is an interesting and important question. The resolution of this issue is essential for a complete understanding of both the proton and nuclear PDFs.

Acknowledgment

We thank Tim Bolton, Janet Conrad, Andrei Kataev, Sergey Kulagin, Shunzo Kumano, Dave Mason, W. Melnitchouk, Donna Naples, Roberto Petti, Voica A. Radescu, Mary Hall Reno, and Martin Tzanov for valuable discussions. F.I.O., I.S., and J.Y.Y. acknowledge the hospitality of Argonne, BNL, CERN, Fermilab, and Les Houches where a portion of this work was performed. This work was partially supported by the U.S. Department of Energy under grant DE-FG02-04ER41299, contract DE-FG02-97IR41022, contract DE-AC05-06OR23177 (under which Jefferson Science Associates LLC operates the Thomas Jefferson National Accelerator Facility), the National Science Foundation grant 0400332, and the Lightner-Sams Foundation. The work of J. Y. Yu was supported by the Deutsche Forschungsgemeinschaft (DFG) through grant No. YU 118/1-1. The work of K. Kovařík was supported by the ANR projects ANR-06-JCJC-0038-01 and Tools-DMColl, BLAN07-2-194882.

-
- [1] J. C. Collins, D. E. Soper, and G. Sterman. Factorization of Hard Processes in QCD. In A. H. Mueller, editor, *Perturbative Quantum Chromodynamics*. World Scientific, 1989.
- [2] J. C. Collins and D. E. Soper. The Theorems of perturbative QCD. *Ann. Rev. Nucl. Part. Sci.*, 37:383, 1987.
- [3] J. C. Collins. Hard-scattering factorization with heavy quarks: A general treatment. *Phys. Rev.*, D58:094002, 1998, hep-ph/9806259.
- [4] : R. D. Ball et al. Precision determination of electroweak parameters and the strange content of the proton from neutrino deep-inelastic scattering. 2009, 0906.1958.
- [5] R. D. Ball et al. A determination of parton distributions with faithful uncertainty estimation. *Nucl. Phys.*, B809:1–63, 2009, 0808.1231.
- [6] A. D. Martin, W. J. Stirling, R. S. Thorne, and G. Watt. Parton distributions for the LHC. 2009, 0901.0002.
- [7] A. D. Martin, W. J. Stirling, R. S. Thorne, and G. Watt. Update of parton distributions at NNLO. *Phys. Lett.*, B652:292–299, 2007, 0706.0459.

- [8] Pavel M. Nadolsky et al. Implications of CTEQ global analysis for collider observables. *Phys. Rev.*, D78:013004, 2008, 0802.0007.
- [9] W. K. Tung et al. Heavy quark mass effects in deep inelastic scattering and global QCD analysis. *JHEP*, 02:053, 2007, hep-ph/0611254.
- [10] P. Jimenez-Delgado and E. Reya. Dynamical NNLO parton distributions. *Phys. Rev.*, D79:074023, 2009, 0810.4274.
- [11] M. Gluck, P. Jimenez-Delgado, and E. Reya. Dynamical parton distributions of the nucleon and very small- x physics. *Eur. Phys. J.*, C53:355–366, 2008, 0709.0614.
- [12] M. Hirai, S. Kumano, and T. H. Nagai. Determination of nuclear parton distribution functions and their uncertainties in next-to-leading order. 2007, arXiv:0709.3038 [hep-ph].
- [13] M. Hirai, S. Kumano, and T. H. Nagai. Nuclear parton distribution functions and their uncertainties. *Phys. Rev.*, C70:044905, 2004, hep-ph/0404093.
- [14] K. J. Eskola, H. Paukkunen, and C. A. Salgado. EPS09 - a New Generation of NLO and LO Nuclear Parton Distribution Functions. *JHEP*, 04:065, 2009, 0902.4154.
- [15] K. J. Eskola, H. Paukkunen, and C. A. Salgado. An improved global analysis of nuclear parton distribution functions including RHIC data. *JHEP*, 07:102, 2008, 0802.0139.
- [16] K. J. Eskola, V. J. Kolhinen, H. Paukkunen, and C. A. Salgado. A global reanalysis of nuclear parton distribution functions. 2007, hep-ph/0703104.
- [17] D. de Florian and R. Sassot. Nuclear parton distributions at next to leading order. *Phys. Rev.*, D69:074028, 2004, hep-ph/0311227.
- [18] J. Gomez et al. Measurement of the A -dependence of deep inelastic electron scattering. *Phys. Rev.*, D49:4348–4372, 1994.
- [19] G. Bari et al. A measurement of nuclear effects in deep inelastic muon scattering on deuterium, nitrogen and iron targets. *Phys. Lett.*, B163:282, 1985.
- [20] A. C. Benvenuti et al. Nuclear effects in deep inelastic muon scattering on deuterium and iron targets. *Phys. Lett.*, B189:483, 1987.
- [21] A. Bodek et al. Electron scattering from nuclear targets and quark distributions in nuclei. *Phys. Rev. Lett.*, 50:1431, 1983.
- [22] S. Dasu et al. Measurement of kinematic and nuclear dependence of $R = \sigma_L/\sigma_T$ in deep inelastic electron scattering. *Phys. Rev.*, D49:5641–5670, 1994.
- [23] U. Landgraf. Nuclear effects in deep inelastic scattering. *Nucl. Phys.*, A527:123c–135c, 1991.
- [24] E. Rondio. Nuclear effects in deep inelastic scattering. *Nucl. Phys.*, A553:615c–624c, 1993.
- [25] H. L. Lai et al. Improved parton distributions from global analysis of recent deep inelastic scattering and inclusive jet data. *Phys. Rev.*, D55:1280–1296, 1997, hep-ph/9606399.
- [26] H. L. Lai et al. Global QCD analysis of parton structure of the nucleon: CTEQ5 parton distributions. *Eur. Phys. J.*, C12:375–392, 2000, hep-ph/9903282.
- [27] J. F. Owens et al. The impact of new neutrino DIS and Drell-Yan data on large- x parton distributions. 2007, hep-ph/0702159.
- [28] S. A. Kulagin and R. Petti. Global study of nuclear structure functions. *Nucl. Phys.*, A765:126–187, 2006, hep-ph/0412425.
- [29] S. A. Kulagin and R. Petti. Neutrino inelastic scattering off nuclei. *Phys. Rev.*, D76:094023, 2007, hep-ph/0703033.
- [30] I. Schienbein, J. Y. Yu, C. Keppel, J. G. Morfin, F. Olness, and J. F. Owens. Nuclear PDFs from neutrino deep inelastic scattering. 2007, arXiv:0710.4897 [hep-ph].
- [31] M. Arneodo et al. Measurement of the proton and deuteron structure functions, $F_2(p)$ and $F_2(d)$, and of the ratio $\sigma(L)/\sigma(T)$. *Nucl. Phys.*, B483:3–43, 1997, hep-ph/9610231.
- [32] P. Amaudruz et al. A reevaluation of the nuclear structure function ratios for D, He, Li-6, C and Ca. *Nucl. Phys.*, B441:3–11, 1995, hep-ph/9503291.
- [33] A. Airapetian et al. Measurement of $R = \sigma_L/\sigma_T$ in deep-inelastic scattering on nuclei. 2002, hep-ex/0210068.
- [34] M. Arneodo et al. The structure function ratios F_2^{Li}/F_2^D and F_2^C/F_2^D at small x . *Nucl. Phys.*, B441:12–30, 1995, hep-ex/9504002.
- [35] J. Ashman et al. Measurement of the ratios of deep inelastic muon - nucleus cross-sections on various nuclei compared to deuterium. *Phys. Lett.*, B202:603, 1988.
- [36] M. Arneodo et al. Measurements of the nucleon structure function in the range $0.002 < x < 0.17$ and $0.2 \text{ GeV}^2 < Q^2 < 8 \text{ GeV}^2$ in deuterium, carbon and calcium. *Nucl. Phys.*, B333:1, 1990.
- [37] M. R. Adams et al. Shadowing in inelastic scattering of muons on carbon, calcium and lead at low x_{Bj} . *Z. Phys.*, C67:403–410, 1995, hep-ex/9505006.
- [38] A. Bodek et al. A comparison of the deep inelastic structure functions of deuterium and aluminum nuclei. *Phys. Rev. Lett.*, 51:534, 1983.
- [39] J. Ashman et al. A measurement of the ratio of the nucleon structure function in copper and deuterium. *Z. Phys.*, C57:211–218, 1993.
- [40] M. R. Adams et al. Saturation of shadowing at very low x_{Bj} . *Phys. Rev. Lett.*, 68:3266–3269, 1992.
- [41] M. Arneodo et al. The A dependence of the nuclear structure function ratios. *Nucl. Phys.*, B481:3–22, 1996.
- [42] M. Arneodo et al. The Q^2 dependence of the structure function ratio F_2^{Sn}/F_2^C and the difference $R^{Sn} - R^C$ in deep inelastic muon scattering. *Nucl. Phys.*, B481:23–39, 1996.
- [43] D. M. Alde et al. Nuclear dependence of dimuon production at 800 GeV. FNAL-772 experiment. *Phys. Rev. Lett.*, 64:2479–2482, 1990.
- [44] M. A. Vasilev et al. Parton energy loss limits and shadowing in Drell-Yan dimuon production. *Phys. Rev. Lett.*, 83:2304–2307, 1999, hep-ex/9906010.
- [45] J. Pumplin et al. New generation of parton distributions with uncertainties from global QCD analysis. *JHEP*, 07:012, 2002, hep-ph/0201195.
- [46] M. A. G. Aivazis, F. I. Olness, and W. K. Tung. Lepton production of heavy quarks. 1) General formalism and kinematics of charged current and neutral current production processes. *Phys. Rev.*, D50:3085–3101, 1994, hep-ph/9312318.
- [47] M. A. G. Aivazis, J. C. Collins, F. I. Olness, and W. K. Tung. Lepton production of heavy quarks. 2) A unified QCD formulation of charged and neutral current processes from fixed target to collider energies. *Phys. Rev.*, D50:3102–3118, 1994, hep-ph/9312319.
- [48] S. Kretzer and I. Schienbein. Heavy quark initiated contributions to deep inelastic structure functions. *Phys. Rev.*, D58:094035, 1998, hep-ph/9805233.

- [49] M. Tzanov et al. Precise measurement of neutrino and anti-neutrino differential cross sections. *Phys. Rev.*, D74:012008, 2006, hep-ex/0509010.
- [50] M. Tzanov. PhD. thesis.
- [51] G. Onengut et al. Measurement of nucleon structure functions in neutrino scattering. *Phys. Lett.*, B632:65–75, 2006.
- [52] J. Botts et al. CTEQ parton distributions and flavor dependence of sea quarks. *Phys. Lett.*, B304:159–166, 1993, hep-ph/9303255.
- [53] H. L. Lai et al. Global QCD analysis and the CTEQ parton distributions. *Phys. Rev.*, D51:4763–4782, 1995, hep-ph/9410404.
- [54] S. J. Brodsky, I. Schmidt, and J. J. Yang. Nuclear antishadowing in neutrino deep inelastic scattering. *Phys. Rev.*, D70:116003, 2004, hep-ph/0409279.
- [55] T. Adams et al. Terascale Physics Opportunities at a High Statistics, High Energy Neutrino Scattering Experiment: NuSOnG. *Int. J. Mod. Phys.*, A24:671–717, 2009, 0803.0354.
- [56] D. Drakoulakos et al. Proposal to perform a high-statistics neutrino scattering experiment using a fine-grained detector in the NuMI beam. hep-ex/0405002.
- [57] T. Adams et al. QCD Precision Measurements and Structure Function Extraction at a High Statistics, High Energy Neutrino Scattering Experiment: NuSOnG. 2009, 0906.3563.